Inline holographic coherent anti-Stokes Raman microscopy

Qian Xu, [1] Kebin Shi, [1] Haifeng Li, [1] Kerkil Choi, [2] Ryoichi Horisaki, [2] David Brady, [2] Demetri Psaltis, [3] and Zhiwen Liu[1,*]

[1]*Department of Electrical Engineering, the Pennsylvania State University, University Park, PA 16802 USA*
[2]*Department of Electrical and Computer Engineering, Duke University, Durham, North Carolina 27708 USA*
[3]*School of Engineering, Ecole Polytechnique Fédérale de Lausanne, Lausanne, Switzerland*
*zliu@psu.edu

Abstract: We demonstrate a simple approach for inline holographic coherent anti-Stokes Raman scattering (CARS) microscopy, in which a layer of uniform nonlinear medium is placed in front of a specimen to be imaged. The reference wave created by four-wave mixing in the nonlinear medium can interfere with the CARS signal generated in the specimen to result in an inline hologram. We experimentally and theoretically investigate the inline CARS holography and show that it has chemical selectivity and can allow for three-dimensional imaging.

OCIS codes: (180.0180) Microscopy; (090.0090) Holography; (300.6230) Spectroscopy, coherent anti-Stokes Raman scattering.

References and links

1. S. A. Benton, and V. M. Bove, Jr., *Holographic Imaging* (Wiley-Interscience, Hoboken, NJ, USA, 2008).
2. H. J. Coufal, D. Psaltis, G. T. Sincerbox, A. M. Glass, and M. J. Cardillo, *Holographic Data Storage* (Springer, New York, NY, USA, 2003).
3. B. W. Schilling, T. C. Poon, G. Indebetouw, B. Storrie, K. Shinoda, Y. Suzuki, and M. H. Wu, "Three-dimensional holographic fluorescence microscopy," Opt. Lett. **22**(19), 1506–1508 (1997).
4. J. Rosen, and G. Brooker, "Non-scanning motionless fluorescence three-dimensional holographic microscopy," Nat. Photonics **2**(3), 190–195 (2008).
5. C. L. Hsieh, R. Grange, Y. Pu, and D. Psaltis, "Three-dimensional harmonic holographic microcopy using nanoparticles as probes for cell imaging," Opt. Express **17**(4), 2880–2891 (2009).
6. Y. Pu, M. Centurion, and D. Psaltis, "Harmonic holography: a new holographic principle," Appl. Opt. **47**(4), A103–A110 (2008).
7. J. X. Cheng, and X. S. Xie, "Coherent anti-Stokes Raman scattering microscopy: Instrumentation, theory, and applications," J. Phys. Chem. B **108**(3), 827–840 (2004).
8. M. D. Duncan, J. Reintjes, and T. J. Manuccia, "Scanning coherent anti-Stokes Raman microscope," Opt. Lett. **7**(8), 350–352 (1982).
9. A. Zumbusch, G. R. Holtom, and X. S. Xie, "Three-Dimensional Vibrational Imaging by Coherent Anti-Stokes Raman Scattering," Phys. Rev. Lett. **82**(20), 4142–4145 (1999).
10. C. Heinrich, S. Bernet, and M. Ritsch-Marte, "Wide-field coherent anti-Stokes Raman scattering microscopy," Appl. Phys. Lett. **84**(5), 816–818 (2004).
11. I. Toytman, K. Cohn, T. Smith, D. Simanovskii, and D. Palanker, "Wide-field coherent anti-Stokes Raman scattering microscopy with non-phase-matching illumination," Opt. Lett. **32**(13), 1941–1943 (2007).
12. K. Shi, H. Li, Q. Xu, D. Psaltis, and Z. Liu, "Coherent anti-Stokes Raman holography for single-shot non-scanning chemically selective three-dimensional imaging," Phys. Rev. Lett., **104**, (2010).
13. A. J. Devaney, "Geophysical Diffraction Tomography," IEEE Trans. Geosci. Rem. Sens. **22**(1), 3–13 (1984).
14. D. J. Brady, K. Choi, D. L. Marks, R. Horisaki, and S. Lim, "Compressive Holography," Opt. Express **17**(15), 13040–13049 (2009).
15. E. Candès, and J. Romberg, "Sparsity and incoherence in compressive sampling," Inverse Probl. **23**(3), 969–985 (2007).
16. J. M. Bioucas-Dias, and M. A. T. Figueiredo, "A new TwIST: Two-step iterative shrinkage/thresholding algorithms for image restoration," IEEE Trans. Image Process. **16**(12), 2992–3004 (2007).
17. Y. R. Shen, *The principles of nonlinear optics* (Wiley-Interscience, New York, USA, 1984).

18. M. Born, and E. Wolf, *Principles of Optics* (Cambridge University Press, Cambridge, England, 1999).
19. J. Van Roey, J. Vanderdonk, and P. E. Lagasse, "Beam-Propagation Method - Analysis and Assessment," J. Opt. Soc. Am. **71**(7), 803–810 (1981).
20. E. Nichelatti, and G. Pozzi, "Improved beam propagation method equations," Appl. Opt. **37**(1), 9–21 (1998).

1. Introduction

Over the past several decades, holography has found a myriad of applications in a variety of areas [1, 2]. Despite its unique ability to record the phase and the amplitude of a wave, the contrast mechanism of an optical holographic image is based on differences in refractive index and absorption and as a result it usually does not have chemical selectivity. Holography has also been applied to fluorescence [3, 4] and second harmonic [5, 6] microscopy which utilize fluorophores or second harmonic nanocrystal markers to provide the contrast. Unlike these imaging modalities, coherent anti-Stokes Raman scattering (CARS) microscopy has been extensively investigated in recent times due to its capability to perform label-free imaging as well as the significantly improved sensitivity of CARS compared to spontaneous Raman scattering [7–11]. We have recently demonstrated a holographic CARS imaging technique which combines the unique ability of both holography and CARS and can perform three-dimensional chemical selective imaging [12]. Briefly, a CARS signal field is first generated in a sample by a pump beam and a Stokes beam. The CARS signal then interferes with a reference wave generated by an optical parametric oscillator to form a CARS hologram. By capturing both the amplitude and the phase of a CARS field holographically, it is shown that three-dimensional imaging can be achieved by digital propagation of the recorded field. Here we report an inline CARS holography method. Specifically, a thin layer of uniform third order nonlinear medium is first placed in front of a specimen to be imaged. When the sample is illuminated with a pump (also used as a probe) beam and a tunable Stokes beam, a reference wave is generated in the nonlinear medium through four wave mixing. The reference and the CARS signal resonantly generated in the specimen by the same pump and Stokes beams can interfere and result in an inline hologram. Main advantages of the proposed technique include that it requires no separate reference beam and that the signal and the reference waves naturally overlap both spatially and temporally. In addition, it is also relatively less susceptible to system instability.

2. Experimental results

The schematic diagram of our experimental setup is shown in Fig. 1. The output at fundamental frequency (λ=1064 nm) from a Q-switched pulsed laser (Continuum Surelite III, repetition rate: 10 Hz, pulse duration ~5 ns, injection seeded) is used as a pump beam for generating CARS signal. The frequency-doubled output from the laser is used to pump a type II optical parametric oscillator (OPO) (Photop Technologies, OPO BBO-2B) to produce a tunable Stokes beam. The two beams are then weakly focused by two lenses with focus lengths of 750 mm and 150 mm respectively and spatially overlapped on a sample. A tunable delay line in the pump beam path can be adjusted to optimize the temporal overlapping. The sample consists of two parts which are sandwiched between three glass slides as illustrated in the inset of Fig. 1. The first part is a thin layer of uniform nonlinear medium, which is used to produce a reference wave through four wave mixing for recording a CARS hologram. In our experiments, index oil (about 10 μm thick) was used. The second part, which is placed behind the nonlinear medium, is the actual specimen to be holographically imaged. The CARS signal generated from the specimen of interest interferes with the reference wave generated in the nonlinear medium. The resulted interference pattern (or inline hologram) is magnified by an imaging system consisting of a long-working-distance objective lens (numerical aperture: 0.42, focal length: 10 mm) and a lens (focal length: 500 mm), and captured by a CCD camera (Apogee 32ME). The undepleted pump and Stokes beams are blocked with a small piece of Teflon. A band-pass filter (Chroma D800/30) is used to further filter out any remaining pump and Stokes beams.
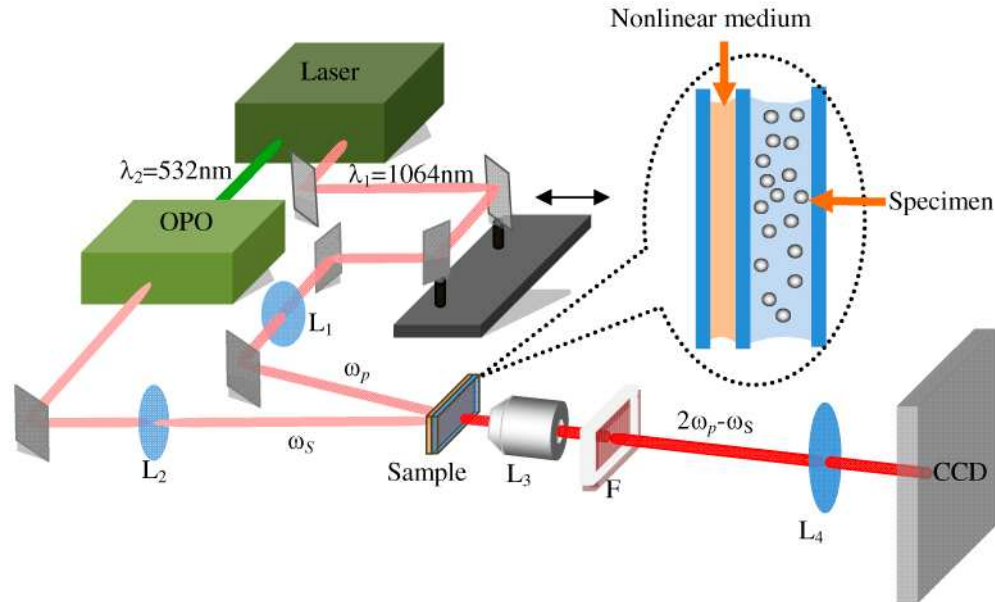
Fig. 1. Schematic diagram of the in-line holographic CARS imaging setup. L_1: lens, focal length 750 mm, L_2: lens, focal length 150 mm, L_3: long working distance objective lens, focal length 10 mm, L_4: lens, focal length 500 mm. As shown in the inset, sample includes a layer of nonlinear medium (index oil) to generate a reference wave and a specimen to be imaged.

We first prepared a specimen consisting of a Poly(methyl methacrylate) (PMMA, Bangs Lab., nominal diameter: 10 μm) and a polystyrene (Duke Scientific, nominal diameter: 10 μm) microspheres immobilized on a cover glass (VWR No.1 cover glass) by UV curable optical adhesive (Norland Optical Adhesive 60). As aforementioned the whole sample was sandwiched between three pieces of cover glasses. Index oil was sealed between the first two cover glasses while the third glass was the one with immobilized microspheres which were immersed in water. Silicone lubricant was used to seal the edges of the glasses to avoid leakage. An optical microscope image of the two microspheres is shown in Fig. 2(a). Then we used our system to record inline holograms of the specimen. The energies of the pump pulse and Stokes pulse were about 8 mJ and 4 mJ, corresponding to peak intensities of approximately 5 GW/cm^2 and 16 GW/cm^2 respectively. The exposure time was 1.5 seconds corresponding to about 15 shots of pulsed exposure. The Stokes beam was first tuned to resonantly excite the vibrational mode of PMMA at 2959 cm^{-1}. A hologram recorded at PMMA resonance is shown in Fig. 2(b). The specimen was defocused during the recording. The hologram was then digitally back-propagated and the reconstruction is shown in Fig. 2(c). We can clearly see that the PMMA sphere is much brighter than the polystyrene sphere. However, the off-resonant polystyrene sphere is also observable and shows focusing/defocusing effect as well during digital back-propagation. This might originate from two reasons: first, the non-resonant four waving mixing background generated by the off-resonance sphere can interfere with the reference wave to record a weak four wave mixing hologram; second, the scattering of the reference wave by the polystyrene microsphere can also result in a Gabor hologram. In order to record a high quality CARS hologram, one will need to suppress the contributions due to both non-resonant four wave mixing background and scattering of the reference wave. We next tuned the wavelength of the Stokes beam to resonantly excite the vibrational mode of polystyrene at 3060 cm^{-1}. The same exposure time and excitation pulse energies were used in the experiment. A hologram obtained at polystyrene resonance is shown in Fig. 2(d). Similarly, the digital back-propagation result as given in Fig. 2(e) reveals that the polystyrene microsphere is much brighter than the PMMA

sphere in this case. These results show that inline holograms with good chemical selectivity can be obtained by our system. It should be noted that nonresonant four wave mixing background can also be generated from surrounding medium (e.g., water, in our case) as well as glass cover slides and could be exploited as a reference wave for recording inline holograms. However, we found that under our experimental conditions such nonresonant background was not strong enough for recording holograms of good quality. Figure 2(f) shows a hologram recorded without the use of a nonlinear layer. As can be seen, the fringes are hardly visible.
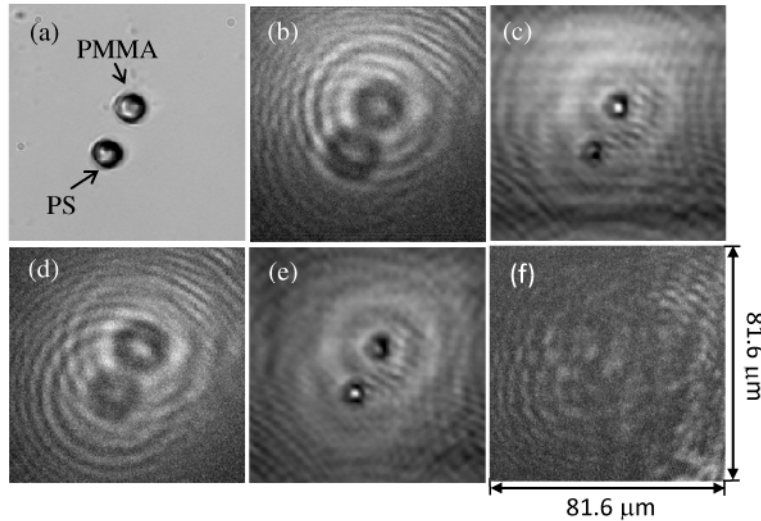

Fig. 2. Chemical selective in-line holographic CARS imaging. (a) an optical microscope image of a PMMA and a polystyrene (PS) spheres; (b) a hologram recorded at PMMA resonance; (c) reconstruction by digital back-propagation showing a resonant PMMA microsphere; (d) hologram recorded at polystyrene (PS) resonance; (e) reconstruction by digital back-propagation showing a resonant PS microsphere; (f) a hologram recorded without the use of a nonlinear layer.

We also experimentally investigated inline holographic imaging of multiple PMMA microspheres suspended in water. During the experiment, the Stokes wavelength was tuned to match PMMA resonance at 2959 cm^{-1}. The energies of pump and Stokes pulses were about 10 mJ and 5 mJ, corresponding to peak intensities of approximately 6 GW/cm^2 and 20 GW/cm^2 respectively. The exposure time was set to 90 ms to ensure single shot exposure. The microspheres were essentially still during the recording as the pulse width of the laser is only about 5 ns. Figure 3(a) shows a recorded hologram, which can be reconstructed by digital propagation. However, it is well known that the reconstructed fields by backpropagation of an inline hologram contain undesirable autocorrelation and twin-image terms. A three-dimensional tomographic reconstruction of an object density may be obtained by using multiple diffracted projections [13]. In general, the twin and the autocorrelation terms may be removed by using optical techniques such as off-axis holography or phase-shifting methods. Brady *et. al.* have recently demonstrated that a three-dimensional tomographic reconstruction may be estimated from a single inline hologram [14] for signals that are sparse in some basis. The technique is called compressive holography, which integrates the concept of compressive sensing [15] and diffraction tomography into digital holography. In addition, for inline holograms, compressive holography can numerically separate the autocorrelation and the twin-image terms from the object signal [14]. Considering these advantages, we have explored the compressive holography technique for reconstructing a CARS hologram. As described in [14], we solved a constrained optimization

problem in which the sparsity prior is enforced by minimizing the ℓ_1-norm of the object estimate. Namely, we solved an optimization problem defined as

$$\hat{f} = \arg\min_{f} \frac{1}{2}\left\|g - 2\,\mathrm{Re}(Hf)\right\|^2 + \tau\left\|f\right\|_1,$$

where

$$\left\|f\right\|_1 = \sum_z \sum_x \sum_y \left|f_{x,y,z}\right|.$$

The matrix H represents the Fresnel propagation operator, f and g denote vectors representing the 3D object density and the 2D measured field, respectively, and τ denotes a regularization parameter which was determined by trial and error. The operator Re extracts the real part of its arguments. To solve the optimization problem, we adapted two-step iterative shrinkage/thresholding algorithm [16]. Figure 3 compares a compressive holography reconstruction to the backpropagation reconstruction created from the recorded CARS in-line hologram, shown in Fig. 3(a). Figures 3(b)-(d) show the axial slices of a backpropagation reconstruction, while Fig. 3(e)-(g) present the axial slices of the associated compressive holography reconstruction. The axial distances are −33 (3 (b) and (e)), −61 (3 (c) and (f)), and −82 μm (3 (d) and (g)), respectively. Clearly, the compressive holography reconstruction suffers much less from the autocorrelation and the twin-image artifacts compared to the backpropagation reconstructions. It should be noted that the bright spots shown in the reconstructions are much smaller than the nominal diameter of the microspheres (10 μm) indicating that the CARS field is focused by the microspheres. To obtain CARS images of microspheres, one can continue the digital propagation of the CARS field until reaching the exit plane of the microspheres [12]. We would like to point out that in general a sample would not always focus the generated CARS field and therefore the compressive holography reconstruction can usually find an estimate closer to the source density of the sample than the diffracted field.
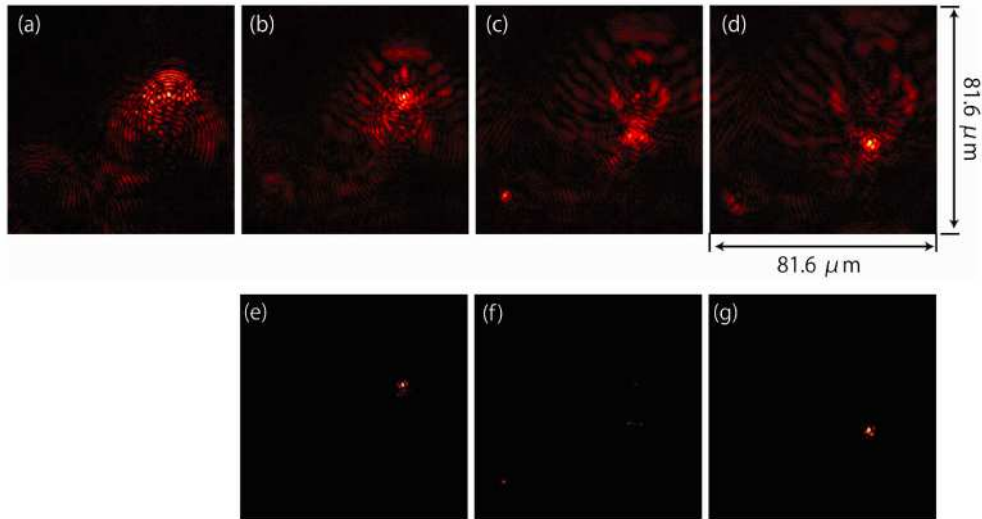

Fig. 3. In-line holographic CARS imaging of multiple PMMA microspheres suspended in water. (a) recorded inline hologram; (b)-(d) digital back-propagation results at different planes; (e)-(g) compressive holographic reconstruction; from (b) to (d) and (e) to (g), z= −33 μm, −61 μm, −82 μm, respectively.

3. Theoretical analysis

To gain additional insight, we investigate theoretically the recording of inline CARS holograms. Under scalar and undepleted pump and Stokes approximation, the anti-Stokes, the pump, and the Stokes fields satisfy the following wave equations respectively [17].

$$[\nabla^2 + \tfrac{\omega_{as}^2}{c^2} n(\omega_{as}, x, y, z)^2] E_{as} = -\tfrac{4\pi\omega_{as}^2}{c^2} \chi^{(3)} E_p^2 E_s^* \qquad (1)$$

$$[\nabla^2 + \tfrac{\omega_p^2}{c^2} n(\omega_p, x, y, z)^2] E_p = 0 \qquad (2)$$

$$[\nabla^2 + \tfrac{\omega_s^2}{c^2} n(\omega_s, x, y, z)^2] E_s = 0 \qquad (3)$$

where $\omega_{as}, \omega_p, \omega_s$ are the angular frequencies of the anti-Stokes, pump, and Stokes beams, c is the speed of light in vacuum, n is the refractive index of the specimen, $\chi^{(3)}$ is the relevant third order nonlinear susceptibility, and E_{as}, E_p and E_s are the anti-Stokes, pump and Stokes fields in the specimen. Assuming small variation of the refractive index, we can rewrite Eq. (1) as:

$$(\nabla^2 + \tfrac{\omega_{as}^2}{c^2} \bar{n}^2) E_{as} = -\tfrac{4\pi\omega_{as}^2}{c^2} \chi^{(3)} E_p^2 E_s^* - \tfrac{\omega_{as}^2}{c^2} 2\bar{n}\Delta n E_{as} \qquad (4)$$

where $\bar{n}$ is the average refractive index and $\Delta n = n - \bar{n}$ is the index variation. The second term on the right hand side of Eq. (4) represents the scattering effect due to a non-uniform linear refractive index distribution. If the specimen is linear, i.e., $\chi^{(3)} = 0$, Eq. (4) describes the scattering of the reference wave and can be rewritten by using Born's approximation [18]:

$$(\nabla^2 + \tfrac{\omega_{as}^2}{c^2} \bar{n}^2) E_{sc} = -\tfrac{\omega_{as}^2}{c^2} 2\bar{n}\Delta n E_r \qquad (5)$$

where E_r denotes the reference wave created by four wave mixing in the nonlinear medium placed in front of the specimen, and E_{sc} is the scattered field. This equation can be solved by using the Green's function. The total field is then given by $E_r + E_{sc}$. As a result, a Gabor hologram can be recorded by capturing the total intensity $|E_r + E_{sc}|^2$. In general, Eq. (4) needs to be solved numerically and the solution consists of both the contribution due to scattering of the reference wave and the anti-Stokes signal generated in the specimen. The recorded intensity distribution is therefore given by $I \propto |E_r + E_{sc} + E_{as}^s|^2$ where E_{as}^s is the anti-Stokes field of interest generated by the specimen. To obtain a genuine CARS hologram, one needs to suppress the contribution due to the scattered field (i.e., $|E_{sc}| << |E_{as}^s|$) since it lacks chemical selectivity. Therefore, weak scatterers and/or a relatively weak reference wave are needed. To better understand the inline CARS holographic recording process, we consider a sample consisting of a 10-μm-thick nonlinear medium with nonlinear susceptibility $\chi_{NM}^{(3)}$, a 160-μm-thick spacer, and a specimen consisting of two 10-μm-diameter microspheres A and B immersed in water (A: lower-left, B: upper-right, c.f. Fig. 4) with identical refractive index of 1.5 and separated by about 14 μm. Further, we assume that microsphere A is on resonance and the ratio of the corresponding third order nonlinear susceptibilities is given by $\chi_{NM}^{(3)} : \chi_A^{(3)} : \chi_B^{(3)} = 1.2:1+j:1$. As aforementioned under our experimental conditions the nonresonant background generated from surrounding medium and glass cover slides are quite weak for recording holograms. For simplicity both the spacer and water are assumed to be linear (i.e. $\chi^{(3)} = 0$) in our model. We applied the beam propagation method [19, 20] to

solving Eq. (1)-(3). The initial pump and Stokes fields were assumed as Gaussian beams. The calculated inline hologram is shown in Fig. 4(a) in which we also added random noise that was comparable to the CCD noise in our experimental measurement. Figure 4(c) shows the reconstruction by digital back-propagation of the theoretical inline hologram. The simulation results qualitatively agree with the experimental results shown in Fig. 2. Our simulation also shows that the generated CARS field is focused by the microsphere, which therefore results in a bright spot much smaller than the size of the sphere itself in the reconstructions shown in Figs. 2-4. We also investigated the recording of Gabor hologram by setting $\chi_A^{(3)} = \chi_B^{(3)} = 0$. In this case, only the scattering of the reference wave is considered. Figure 4(b) shows the calculated Gabor hologram while the reconstruction is shown in (d). Clearly, it lacks chemical selectivity as both microspheres have the same brightness. Note that microsphere B appears darker in Fig. 4(c) than in (d), suggesting a destructive interference between the scattered field and the four wave mixing field.
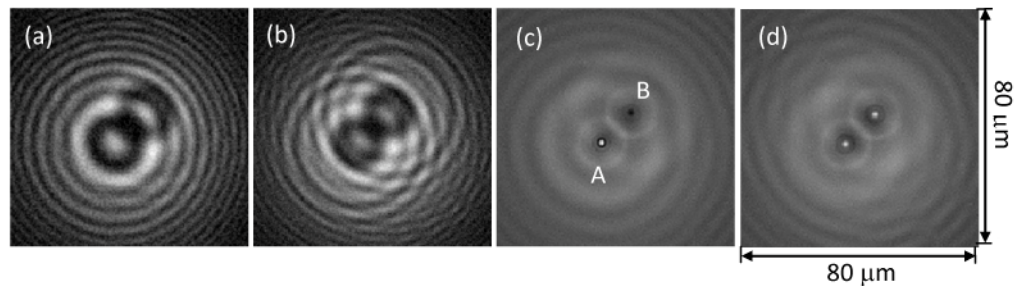

Fig. 4. Theoretical simulations. (a) calculated inline CARS hologram when sphere A is on resonance; (b) calculated Gabor hologram when only scattering effect is considered; (c) digital reconstruction of the inline CARS hologram shown in (a); (d) digital reconstruction of the Gabor hologram shown in (b);

4. Discussion

In summary, we have demonstrated and investigated a simple method for inline CARS holography. It is shown that the recorded inline CARS hologram has good chemical selectivity and that three-dimensional imaging can be achieved by digitally propagating the hologram. We also applied the compressive holography technique to reconstruct the recorded inline hologram, which can significantly suppress the twin image background. However, we should note that the existence of a scattered reference field leads to a superposition of inline CARS hologram with Gabor hologram, and therefore reduces the chemical selectivity. The scattered field could interfere destructively or constructively with the CARS signal generated in the specimen to result in non-uniform image intensity. In addition, the scattered field could also interfere constructively with nonresonant four wave mixing background by lucky phase matching while interfering destructively with resonant CARS signals generated at certain locations, which can potentially result in enhanced background and difficulty in interpreting the results. These limitations can be overcome by generating the reference wave off axis to avoid its propagation through the specimen and hence the recording of a Gabor hologram. Nevertheless, the technique described here is simple to implement and is relatively robust against system instability due to the fact that both the reference and signal are generated by the same pump and Stokes beams and co-propagate in the same media. It can be a useful technique for relatively thin samples (compared to the coherence length of CARS processes) or when combined with other techniques which can suppress the nonresonant background.

Acknowledgement